Electrochimica Acta 494 (2024) 144453

Contents lists available at ScienceDirect

Electrochimica Acta

journal homepage: www.journals.elsevier.com/electrochimica-acta

Photo-induced processes on ZnO and its possible impact on cathodic delamination of organic coatings on galvanised steel

Anna Aspalter [a,b,*], Roland Braidt [b], Jiri Duchoslav [c], Bernhard Strauß [b], Günter Fafilek [a]

[a] TU Wien, Institute of Chemical Technologies and Analytics, Getreidemarkt 9, 1060 Vienna, Austria
[b] voestalpine Stahl GmbH, voestalpine-Straße 3, 4020 Linz, Austria
[c] Center for Surface and Nanoanalytics (ZONA), Johannes Kepler University Linz, Altenbergerstraße 69, 4040 Linz, Austria

ARTICLE INFO

Keywords:
Zinc passive layers
Photoelectrochemistry
Atmospheric corrosion
Oxygen reduction
Organic coatings

ABSTRACT

The influence of sunlight on cathodic delamination of polymer-coated, galvanised steel is considered regarding the semiconductor properties of zinc passive layers. Zinc and galvanised steel were studied potentiostatically in O_2-rich, moderate alkaline electrolyte under UV-, violet and green light. Currents increased instantaneously, intensity- and wavelength-dependant according to the photoeffect. After electrolyte preconditioning of galvanised, pre-treated and coated (6 μm) steel, light positively shifted the open-circuit-potentials (ocp). Mechanistic considerations are provided using Mott-Schottky-plots and Chopped Linear Sweep Voltammetry (CLSV). Under certain conditions, oxygen reduction reaction (ORR) intensification is found and should be considered in future studies of paint adhesion on zinc.

1. Introduction

Polymer coated galvanised steel sheets are often used in outdoor constructions where they are exposed to high levels of UV-light, moisture and temperature. A common failure mechanism as a result of environmental stress is cathodic delamination between polymer and zinc coating [1–3]. There is broad consensus that cathodic delamination is the result of the formation of a galvanic cell: when the coating is damaged, direct contact is created between the metallic substrate and the environment. The metal acts as an anode and the coupled cathodic reaction occurs at the polymer/metal interface, following a delamination front away from the initial defect. In a pH range of 4–11, the ORR dominates the cathodic reaction [1,4,5].

The ORR can occur in a 4 e^- (Equ. 1) or in 2 e^- steps (Eqs. 2 and 3) [6], and as well in a competition of (Eq. 1) and (Eqs. 2 and 3) [7,8].

$$2\,H_2O + 4\,e^- + O_2 \rightarrow 4\,OH^- \quad (1)$$

$$H_2O + 2\,e^- + O_2 \rightarrow HO_2^- + OH^- \quad (2)$$

$$HO_2^- + H_2O + 2\,e^- \rightarrow 3\,OH^- \quad (3)$$

All (Eqs. (1)–(3)) lead to an increase in pH, which is considered detrimental for adhesion according to the early studies of Leidheiser et al. due to substrate and polymer attack [9]. In addition, peroxide species generated in (Equ. 2) contribute to the delamination process through polymer degradation [7].

In corrosion studies, it is assumed that the coated substrate is primarily affected by moisture, so organic coatings have been extensively studied on their water uptake, to describe their corrosion protection. Organic coatings have as well been assessed through their resistance to UV-light [10,11] and to a combination of humidity and UV-light in both accelerated weathering [11–15] and in outdoor exposure [13–15]. However, it has not yet been considered that the UV-light might contribute to reactions at the interface of a coated sample. This seems though of great interest, as ZnO is a semiconductor, with a bandgap of 3.3 to 3.4 eV at room temperature [16–18] just at the edge of the energy of visible light to UV-light, therefore provided by sunlight. In this context the question arises, whether the photoeffect on ZnO (Eq. 4) might contribute to the cathodic delamination of organic coated galvanised steel as a consequence of contribution to the ORR via (Eq. 1) and (Eqs. 2 and 3).

$$ZnO \xrightarrow{h\nu} ZnO + h\cdot + e' \quad (4)$$

The photocathodic protection of steel [19–23] and zinc substrates [22,24,25] by semiconducting materials such as TiO_2 and ZnO is well researched. However, also without paint, the detrimental effects of light on zinc corrosion are less well studied and seem contradictory. This

* Corresponding author.
E-mail addresses: anna.aspalter@tuwien.ac.at, anna.aspalter@outlook.com (A. Aspalter).

https://doi.org/10.1016/j.electacta.2024.144453
Received 11 January 2024; Received in revised form 26 April 2024; Accepted 16 May 2024
Available online 17 May 2024

refers to the fact, that some mechanisms propose photo-contribution to the anodic and others to the cathodic reaction:

Spathis and Poulios [26] performed white light illumination on anodically produced ZnO films on Zn in 3.5% NaCl and found different behaviour depending on anodization time and thus thickness. For thin oxides, illumination led to a higher corrosion rate, while for thicker oxides a protective effect was observed by promoting the formation of the more stable zinc oxychlorides. Illumination also resulted in pitting corrosion, a shift in corrosion potentials to more negative values, and current densities to more positive values. This was attributed to the photocurrent.

In [27], Rudd and Breslin studied zinc under the influence of light from 200–900 nm in borate solution at pH 13. As a result of illumination, both a 10 mV decrease in ocp and an increased anodic current were observed, which was interpreted as dissolution of the passive layer. The effect was explained by the reaction of the photogenerated holes with ZnO according to Equ. 5.

$$ZnO + 2h\cdot \rightarrow Zn^{2+} + \tfrac{1}{2}\, O_2 \quad (5)$$

On the other hand in [28], Juzeliunas et al. investigated the ocp on a 10 μm thick ZnO layer on Zn in 5% NaCl under laser illumination with λ=387 nm. The authors derived the increase in ocp and the increase in cathodic current from an enhanced ORR. They did not find an effect on the anodic reaction and reported the photo-acceleration as part of a combined effect, which then changes to a photoinhibition effect [29].

In [30] various zinc alloys were studied under water immersion and illumination by UV fluorescent lamps. This resulted in higher weight loss and more negative flat band potentials for pure Zn in contrast to natural illumination. The observation was interpreted as transfer of photo-generated electrons to the electrolyte contributing to the ORR.

In [22] Sun et al. attributed non-sufficient protection of illuminated ZnO to Zn to the more negative ocp value of Zn in contrast to the ocp of ZnO. In this case the electrons cannot be transferred to the metal, but undergo reactions with oxygen dissolved in the solution, whereas the holes trap electrons from the metallic substrate and cause dissolution. This is shown by positive ocp shifts in 3.5% NaCl during white light illumination.

In [24] Li et al. obtained as well a positive ocp shift on ZnO in 3.5% NaCl during illumination with artificial sunlight. Here however, this was interpreted as protection effect of the zinc substrate through electron transfer to the substrate. The cathodic reaction was assumed to be the ORR, while the anodic behaviour consisted of zinc dissolution and electron/hole pair generation through illumination. They further observed an enhancement of this effect on samples of electrodeposited nanocrystalline zinc [25].

Nazarov et al. performed SKP-SPV measurements on Zn/ZnO samples during illumination (400–700 nm) in air with varying residual moisture. The illumination decreased the Volta-Potential on Zn/ZnO (180 nm), which was explained by electrons and holes generated by the photoeffect and separated in the surface space charge layer of the semiconductor. In this experiment though, no O_2-containing electrolyte was present. Further, the authors found through SKP potentiometry and polarization techniques, that electrons can be transferred from a Zn/ZnO electrode to the redox system of $[Fe(CN)_6]^{3-}/[Fe(CN)_6]^{2-}$. This effect was solely observed on ZnO layers of 150 nm but not on thin native ZnO layers of 3–4 nm. The chosen Fe^{2+}/Fe^{3+}-cyanide redox couple was stated to model the more complicated ORR. The observation was traced back to the semiconducting properties of ZnO. In the last described measurements however, no illumination was involved [31].

The intention to address the photoelectrochemical behaviour of ZnO to cathodic delamination requires to restudy the poorly conceived contribution of the photoeffect on ZnO to the ORR. This is aimed in this work through conducting a systematic study in terms of wavelength and intensity variation on pure zinc and zinc alloys. Further, investigations on primer coated samples under illumination are performed to establish a relation between photoelectrochemical processes on the substrate and cathodic delamination. Mechanistic considerations are given using flatband potential values and results of CLSV.

2. Material and methods

2.1. Electrochemical setup

All electrochemical measurements were performed in a three-way electrode cell, consisting of the sample as working electrode, an Ag/AgCl ($c_{KCl} = 3$ M) electrode as reference electrode E_{ref} (0.210 V vs. SHE) and a platinum wire as counter electrode. An Interface 1000™ of Gamry Instruments was used as potentiostat. The sampling rate was set to 1 s in potentiostatic and ocp measurements and to 0.1 s in CLSV measurements. A sodium hydrogencarbonate (≥99%, Carl Roth) solution of 10 g/L (M = 84.01 g/mol) with a pH of 8.47 (22.7 °C) was used.

The cell setup was self-designed and 3D-printed with acrylonitrile styrene acrylate. It envolumes 100 ml of the electrolyte and holds a quartz rod as lightguide to prevent absorption or scattering by air or the electrolyte. The sample area is shaped and sized as the light-guide area and has a diameter of 10 mm. The light source sits directly on top of the light guide, which is placed approximately 2 mm above the sample surface.

Three different high-power LEDs served as light sources. The UV LED (LZ1–00UV0R, OSRAM - LED Engin), violet LED (LZ1–00UB0R, OSRAM - LED Engin) and green LED (LZ4–40G108, OSRAM - LED Engin) have peak wavelengths of 365 nm, 405 nm and 525 nm and can be operated in a similar radiant power range according to the specification (UV: 1360 mW, violet: 1260 mW and green: 640 lm at an LED forward current of 700 mA). However, the green LED has a bigger emitting area, thus bigger dimensions of the covering lens and a significant higher beam angle. This issue is successfully compensated by using a lightguide larger than the diameter of the lens in perspective. The number of photons/s impinging at the sample surface in air environment was measured with a Si photodiode (S120VC, Thorlabs) and a neutral density filter (MidOpt® ND300) for the green LED and the violet LED. Due to the very similar properties, the photon flux of the UV LED was estimated by the characterization of the violet LED. This assumption seems justified since, according to the fabricant, the photonflux of the UV light makes up 91–98% of the photon flux of the violet light in the range between 300 and 900 mA. Further, it seems a better approach than experimental determination as the transmittance of the available ND filter was too low for UV-light. It shall be mentioned here that the absolute values of specified photon fluxes might be inaccurate, however it could be shown independently from the fabricants data that the operation ranges of the violet and green LED overlap.

For continuous illumination, the LEDs were powered in constant current mode by a power supply (BASETech BT-305 and velleman LABPS3005DN), while assuring the pre-set forward current of the LEDs stayed at constant value by using an LED driver (RECOM RCD-24–1.00). In addition, the forward current was measured with an amperemeter in series. For light chopping as in linear sweep voltammetry an LED light controller (Gardasoft, RC120) was used.

2.2. Sample preparation

99.99% pure zinc samples ($Zn_{99.99\%}$) and different industrial substrates (hot dip galvanised steel samples: Z275, ZM120, Z100), the latter provided by voestalpine[2], were studied. Samples denoted as Z275, ZM120 and Z100 constitute zinc-coated steel panels with a coating thickness of 20 μm, 9 μm and 7 μm. Z275 and Z100 samples are produced from a zinc bath, which contains less than 1 w% of aluminium, whereas for ZM120 samples a zinc bath with approximately 2.5 w% of aluminium and 1.5 w% of magnesium is used. Additionally, surfaces of Z275 and ZM120 are skin-passed, which is a common surface preparation for subsequent paint coating steps. Z100 in contrast is not skin-

passed.

Prior to all measurements, samples of $Zn_{99.99\%}$ where grinded with sandpaper (P1200) and polished with diamond pastes of 3 μm and 1 μm grain sizes to mirror finish. Industrial samples, were cleaned by spraying with an alkaline solution (Bonderite C-AK C72, Henkel) at pH 11 and 40 °C for 24 s in two separate sections to remove anticorrosive oils and slightly etch the surface.

For the ocp measurements on organic coatings, the samples were prepared as follows: steel panels with Z275 coatings were cleaned by the above-described cleaning step, pre-treated with a commercially available chromate free solution (Bonderite M-NT 1455T, Henkel) via immersion of 5 s at 35 °C, which creates a conversion layer of ~ 100 nm and coated with a polyurethane-based primer. This commercial primer contains TiO_2 pigments and inorganic anticorrosive pigments. It was temperature-crosslinked (at a PMT of 235 °C) and the thickness of the coating was about 6 μm.

2.3. Characterization of the layers

Field Emission SEM was performed using the ultra 55 equipment (Zeiss) with an Inlens detector. The excitation voltage was set to 5 kV. The cross-sections were prepared via cross-section-polishing (CSP) with an Ar beam. To protect the layer to be analysed and for contrast visualization, the sample was painted with a felt-tip pen.

XPS measurements were performed using the NEXSA G2 system (Thermofischer). The acquired spectra were assessed by means of the Avantage software package provided by the system manufacturer. Samples were probed by monochromated Al-Kα X-Ray radiation (1486.6 eV), which was focused to a spot with 400 μm in diameter. The hemispherical analyser was operated in a constant analyser energy mode with a pass energy of 20 eV and energy step of 0.05 eV step for high resolution spectra. The surface charge was compensated with a standard dual flood gun, which provided simultaneously a beam of low energy electrons and Ar ions. Standard charge shift referencing of the spectra via a C1s peak of adventitious carbon at 285.0 eV was applied.

2.4. Potentiostatic measurements

For potentiostatic measurements, the electrolyte was bubbled with O_2 for approximately 5 min with a stream of 2–3 l/h. The measurements shown in Figs. 2 and 3, as well as the raw data of Fig. 6 are the result of a three-sequence protocol. In the first sequence, the potential was set to −1.25 V vs. E_{ref} for 250 s. In this step, the surfaces of the samples were activated due to reduction of the Zn-passivation layer, which shortly forms after being brought in contact with the electrolyte. After that, the open circuit potential was measured for 10 s. The ocp did not reach a constant value within this time. In the third sequence, the potential was set to −1.05 V vs. E_{ref} for 600 s. Within this sequence, the light was switched on every 50 s for approximately 10 s, starting at 100 s and 900 mA LED forward current. In the following periods of light exposure, the forward current was decreased in 100 mA steps to 800, 700, 600, 500, 400, 300, 200 and 100 mA.

2.5. Ocp measurements

Prior to ocp measurements the coated samples were conditioned in the electrolyte for 3 h and 114 ± 2.5 h. A droplet of the electrolyte was positioned solely on the centre of the coated samples to assure the metal edges of the samples were not in contact with the liquid electrolyte. By continuous refill, the droplet was prevented from vaporization. After that, the open circuit potential was measured over a period of 4000 s, while three periods of light experiments with 5 repeats each were done. Period 1, 2 and 3 started at 1000, 2000 and 3000 s. Fig. 7. shows period 2 with light onset at 2000, 2050, 2100, 2150 and 2200s and a duration of 10 s at a forward current of approximately 700 mA.

2.6. Mott-Schottky measurements

The electrolyte was first bubbled with an O_2 flow of 2–3 l/h for 5 min. The samples were prepared in the 3 sequences already described: 1. −1.25 V vs. E_{ref} for 250 s, 2. Ocp for 10 s, 3. −1.05 V vs. E_{ref} for 100 s. The electrical impedance spectra were then recorded on at least 4 replicates at 100 Hz between −0.85 V and −1.15 V vs. E_{ref}. A voltage of 10 mV_{rms} was selected. The sweep rate was set to 15 mV/s for Z275, ZM120 and Z100 and needed to be decreased to 5 mV/s for $Zn_{99.99\%}$, to fit a linear section. The double layer capacitance of the electrolyte is assumed to be remarkably high, so if connected in series with the capacitance of the space charge layer, the latter dominates the capacitance.

2.7. Chopped linear sweep voltammetry

The electrolyte used for CLSV was bubbled with an O_2 stream of 2–3 l/h for 5 min. Afterwards, the sample was set to a potential of -0.85 V vs. E_{ref} (−0.80 V vs. E_{ref} for $Zn_{99.99\%}$) for 900 s to create in situ oxides on the surface. At least 3 replicates were conducted. The linear sweep was performed in a range of -0.85 V to -1.75 V vs. E_{ref} (-0.80 V to −1.7 V vs. E_{ref} for $Zn_{99.99\%}$) with a sweep rate of 0.5 mV/s. During the measurement, the light was chopped. The forward current was set to 700 mA for all three LEDs, the pulse width to 0.1 s and the retrigger time to 1 s.

3. Results and discussion

3.1. Characterization of the layers

SEM and XPS were performed on $Zn_{99.99\%}$, Z275, ZM120 and Z100 after the preparation of the layers via a 3-sequence-protocol: 1. −1.25 V vs. E_{ref} (250 s), 2. ocp (10 s) and 3. −1.05 V vs. E_{ref} (300 s).

Top-view SEM revealed few islands of μm-sized crystals surrounded by a homogenous layer. Since the quantum efficiency of the homogenous layer can be regarded extremely high in relation, its characterization was the main focus. A cross-section on Z100 after CSP preparation within the homogenous area revealed an incompact layer with a thickness of approx. 300 nm (Fig. 1.b).

XPS was performed within the homogenous layers. Table S1 in SI lists the obtained peaks, their respective binding energies and atomic concentrations of chemical states from high resolution spectra. For Z100, the high resolution spectra are given as an example in Fig. S.1 in SI.

On $Zn_{99.99\%}$, Z275, ZM120 and Z100 metallic zinc signal was obtained as well, which is in accordance with the presence of a diffuse layer. Approximate Zn/Al surface ratios can be derived from the Zn2p3/Al2p ratio, which is 31/1 on Z275 and 28/2 on Z100 (in at%). The occurrence of Al was assigned to a pure oxidized form on Z275 and Z100. On ZM120, no Al signal distinguishable from noise was detected with XPS. A ratio of Zn2p3/Mg2p = 17/6 (in at%) is obtained. The scans of ZnLM2 and MgKLM1 were used to derive atomic fractions of Zn or Mg in metallic and non-metallic form. The non-metallic fractions are further given in $ZnO/Zn(OH)_2$ and $ZnCO_3$ contents or respectively MgO or $Mg(OH)_2$ (see Table 1).

As it can be seen ZnO, $Zn(OH)_2$ and $ZnCO_3$ can be found on the samples surfaces in different ratios. While ZnO is the predominant form on $Zn_{99.99\%}$, $Zn(OH)_2$ can be found to the most extent on Z100 and Z275. On ZM120 the occurrence of $Zn(OH)_2$ and $ZnCO_3$ is equivalent in terms of quantity. The presence of photoactive species like Al_2O_3 and MgO does not contradict the work carried out in this study, as their band gaps are significantly higher [32–34].

3.2. Potentiostatic measurements

As a first approximation, it is assumed here, that the current just below the ocp can be directly attributed to the ORR. The validity of this assumption is discussed later. Fig. 2 shows the evolution of the current density during potentiostatic condition (−1.05 V vs. E_{ref}) on $Zn_{99.99\%}$

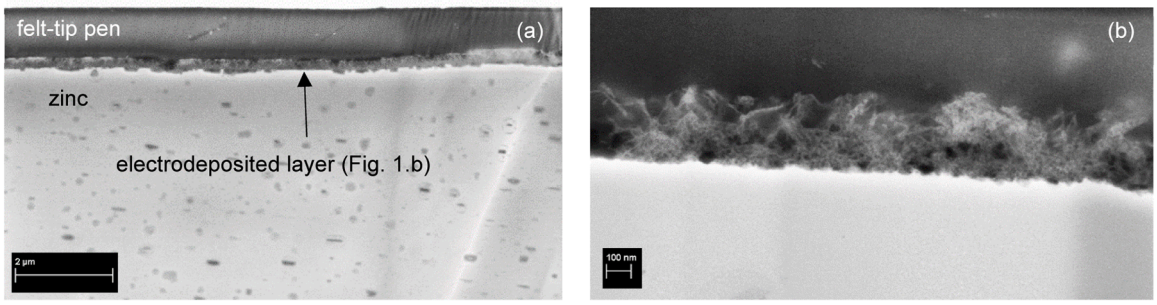

Fig. 1. SEM images of a cross-section of Z100 after electrochemical deposition at −1.05 V vs. E_{ref}: (a) overview, (b) detail.

Table 1
Distribution of non-metallic Zn- or Mg-signal.

Content /%				
	$Zn_{99.99\%}$	Z100	Z275	ZM120
ZnO	52	20	13	16
$Zn(OH)_2$	30	56	77	41
$ZnCO_3$	18	24	10	43
MgO	–	–	–	20
$Mg(OH)_2$	–	–	–	80

over time. The current density is calculated by relating the measured current to the geometric sample area of 0.785 cm^2 in all shown results. As it can be seen on the left parts of Fig. 2.a–c the current density starts in the positive region, indicating the oxidation of zinc to be prevalent at the beginning. The current density then begins to fall and follows a Cottrell curve with the square root of time, as the rate of the anodic oxidation of metallic zinc decreases.

Within this period ZnO, $Zn(OH)_2$ and $ZnCO_3$ forms on the surface, as confirmed by XPS. This is followed by the current density stabilizing at a negative value between −10 and −20 µA/cm^2, which is assumed to be the ORR taking place on the oxidized surface. After a constant value of current density was reached, the light was switched on and off in periodic intervals, highlighted in colour in Fig. 2.a–c. When UV-light (Fig. 2.a) or violet light (Fig. 2.b) is provided, a significant and instantaneous increase of the cathodic current density can be observed. The influence on the current density, which occurs without time delay, clearly indicates a process involving photons and it cannot be explained exclusively by temperature processes [35]. When conducting the experiment with green light (Fig. 2.c), in contrast, no comparable instantaneous impact on the current density can be observed. These findings are in accordance with the fact, that the band gap of ZnO best matches with the energy of the UV light. With violet light, thus light of higher wavelength and lower energy respectively, the effect starts to reduce (see Fig. 2.b), and it nearly fully disappears with green light of even lower energy. (Details of green light triggered effects are presented in Fig. 5). That an effect is observed with violet light indicates that the bandgap of ZnO on the regarded samples is slightly smaller compared to the bandgap value documented in the literature, which usually refer to monocrystalline and very pure samples. The absence of distinct band gap values on passive layers is stated in Burleigh's work due to additional energy levels within the band gap [36].

Also, when switching off the light, an instantaneous reaction can be observed, as the current density abruptly changes back to the curve progression right before the light exposure. Both the instantaneous impact on the current density, as well as the wavelength dependency point out, that the observed phenomenon is linked to the photoeffect: Absorbed photons with energies equal or higher than the bandgap, lift electrons from the valence band into the conduction band, while holes remain in the valence band. Both electrons and holes are available for further reactions with virtually zero time shift. In addition, the characteristic overshoots of the photoelectric effect are found when the light source is switched on and off. The increase in the cathodic current indicates the direct contribution of the photons to a reaction process at the sample, possibly the ORR, as assumed in [28–30]. The decrease of the effect with higher wavelengths suggests a lower number of electrons overcoming the bandgap, being available for reaction contribution.

In addition to the instantaneous effect, there are also slow modulations in the current density signals at all wavelengths. Within the light period the cathodic current density starts to decrease continuously. This trend approximately holds on for the subsequent 15 seconds. It is likely that this finding is due to temperature changes in both the semiconductor and the LED. Both could have an effect on the current density. During the operation of the LED at high power, it heats up, which shifts the LED spectrum to higher wavelengths and reduces the total photonflux. This effect reduces the number of generated electron-hole pairs and therefore the current density as well. Unlike the photogenerated charge carriers, which are only available when the light is on, the LED heats and cools the sample with a delay to the illumination periods, causing the number of thermally generated electron-hole pairs to increase and decrease accordingly. In the case of green light, the effect of temperature is practically the only cause of changes in cathodic current density.

Accordingly, the influence of UV radiation in the solar radiation spectrum range [37] and also the increased temperature are important parameters with outdoor material degradation on ZnO. That temperature achieves a much smaller effect is supported by photoelectrochemical studies of zinc [24,30], where IR radiation was stated to be of minor importance.

Performing the same experiment on Z275 as on $Zn_{99.99\%}$, led to equivalent results, which are shown in Fig. 3. Again, illumination causes both an instantaneous and a delayed effect on the current density during potentiostatic polarisation (−1.05 V vs. E_{ref}). Like on $Zn_{99.99\%}$, current steps are the highest when using UV-light (Fig. 3.a), lower when using violet light (Fig. 3.b) and nearly disappear when using green light (Fig. 3.c).

Proving the causal relation between the observed phenomenon and the photoeffect, can be done through the variation of the cause (light) and the evaluation of changes in effect (current). The variation of the cause (light) can be conducted in terms of wavelength variation, as presented so far, and in terms of intensity variation. Authors in [35] advised as well combined wavelength variation at constant flux and intensity variation at constant wavelength for the proof of photoeffects at gas/solid interfaces. Thus, it can be assumed that a decrease in photon intensity will cause a decrease in current change. For that reason, the photon flux of the illumination periods is reduced as the experiment duration progresses by reducing the forward current of the LEDs in 100 mA steps, starting at 100 s with 900 mA (see Fig. 2 and Fig. 3).

The absolute current steps of the measurements in Figs. 2 and 3 are shown in dependence of the photonflux in Fig. 4.a for $Zn_{99.99\%}$ and in Fig. 4.b for Z275. The current changes, when using green light stays around zero, though its photonflux exceeds the photonflux of the UV-light and violet light. Regarding the data for the UV-light and the

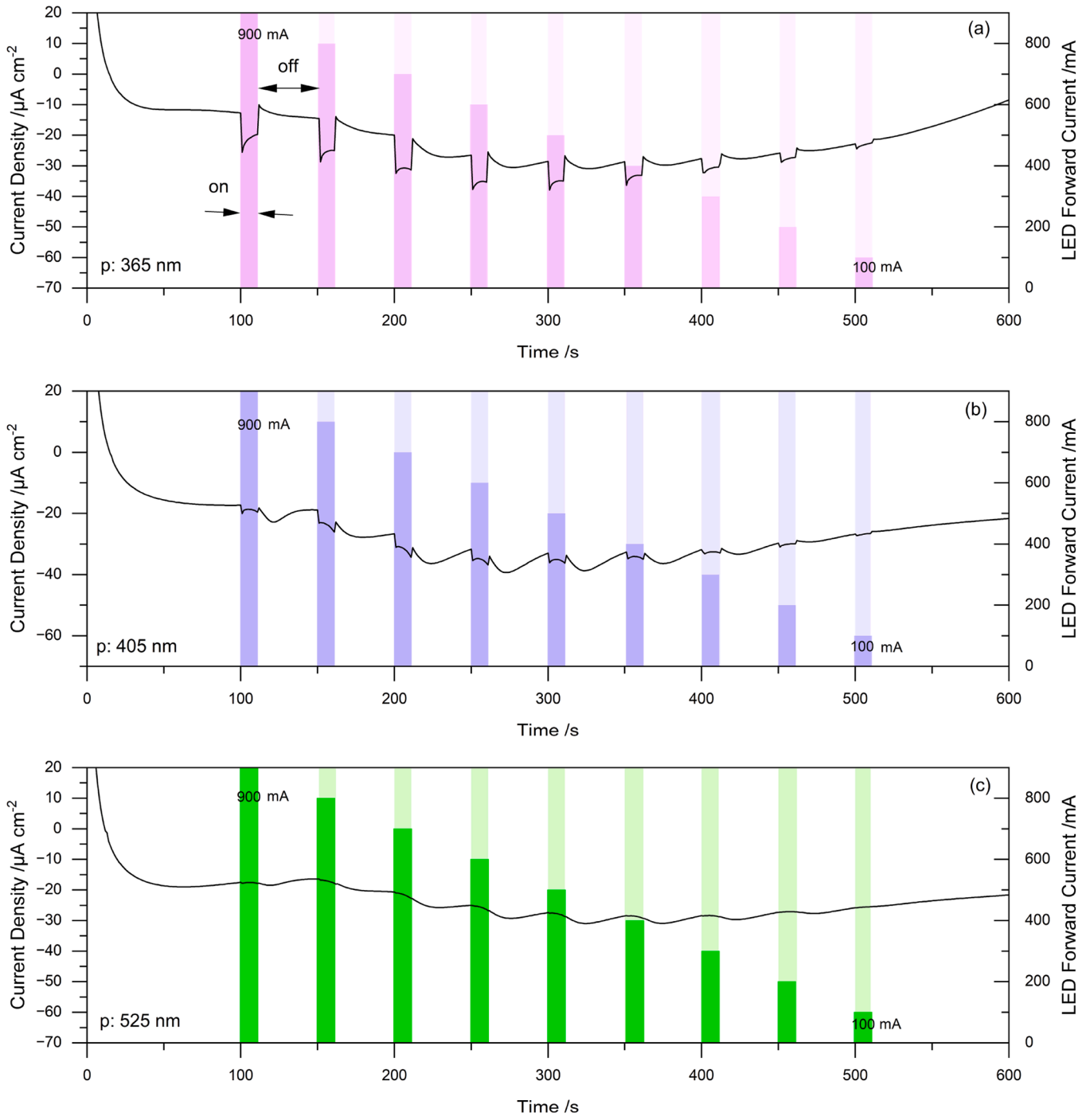

Fig. 2. Current density under potentiostatic condition (−1.05 V vs. E_{ref}) on $Zn_{99.99\%}$ during illumination with the UV (a), violet (b) and green (c) LED with decreasing forward current I_F (900–100 mA) over time.

violet light in Fig. 4.a and b, a linear dependence between the photonflux and the current step is observed until a saturation level is reached at higher photonfluxes. For Z275 this photonflux level is slightly below $4.5 \times 10^{16}\, s^{-1}$ (corresponding to a LED forward current of 600 mA) (see Fig. 4.b), whereas for $Zn_{99.99\%}$ the saturation is at around $5.2 \times 10^{-16}\, s^{-1}$ for violet light (forward current of 700 mA) or $5.8 \times 10^{-16}\, s^{-1}$ for UV-light (forward current of 800 mA) (see Fig. 4a).

In order to evaluate the physical relations, the electron count was plotted against the photon count for both $Zn_{99.99\%}$ (see Fig. 4.c) and Z275 (see Fig. 4.d). For calculating the electron count, Eq. 6 was used, in which e is the elementary charge. The exact value of e [38] was rounded to 1.602×10^{-19} C for calculations. The additional charge ΔQ has been evaluated by integrating the current during illumination between t_1 and t_2 against a straight baseline.

$$\text{Electron count} = \Delta Q \Big/ e = 1 \Big/ e * \left| \int_{t_1}^{t_2} I(t)\mathrm{d}t \right| \tag{6}$$

This is shown in Fig. 4.e as an example for the illumination experiment with violet light at 800 mA forward current on $Zn_{99.99\%}$. The baseline depicts the assumed curve progression without light exposure.

As the characterization of the LEDs revealed an almost linear relation between the forward current and the power, it seems relevant to discuss the occurrence of the saturation. Possibly, the saturation is linked to the

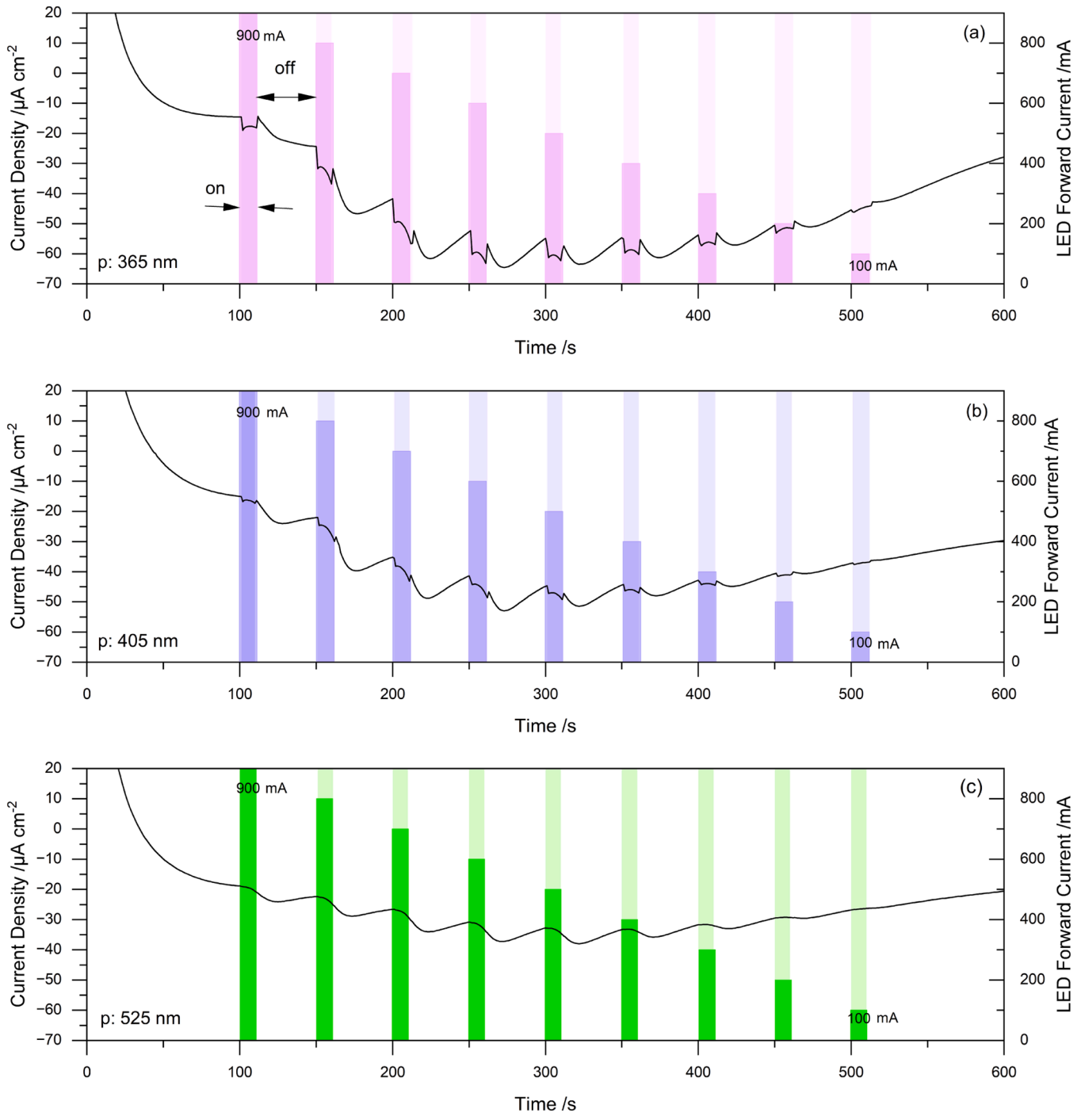

Fig. 3. Current density under potentiostatic condition (−1.05 V vs. E_{ref}) on Z275 during illumination with the UV (a), violet (b) and green (c) LED with decreasing forward current I_F (900–100 mA) over time.

maximum charge carrier concentration of ZnO, which forms a limitation and is closely related to recombination rate and therefore defect concentration.

ZnO is a wide band-gap semiconductor with intrinsic n-type behaviour [16]. It is outdated that native donors as $Zn_i^{\cdot\cdot}$ and $v_O^{\cdot}$, are the main contributors, in fact, semiconducting properties have been attributed to H impurities and their role as background donors and to Zn-interstitials in form of complexes [39]. In general, Al impurities, might contribute to the n-type behaviour as well. The maximum n-type carrier concentration of electrons in ZnO is stated to be in the range of 10^{20} e^-/cm^3 [16], which is in line with Mott-Schottky measurements on pure zinc in [27] and on zinc substrate passive layers in [40]. This would mean that the present ZnO layer in our experiments on $Zn_{99.99\%}$ has a maximum thickness of 70 nm, which seems plausible (determined for the illumination experiment with UV light at 800 mA, saturation at 5.7×10^{14} e^-). This calculation is based on the assumption of a dense layer and consequently might differ from the measured layer thickness as on Z100 (~300 nm), which was found to be diffuse and incompact.

Table 2 shows the slopes obtained by linear fit of the data in Fig. 4.c and d. From this, the ratios between additional consumed electrons and provided photons can be obtained. On $Zn_{99.99\%}$ 970 photons (p: 365 nm) are needed for the consumption of 1 additional electron. This value rises to 1700 photons (p: 365 nm) on Z275. The obtained results with the UV light are in good accordance with measurements from [36], where

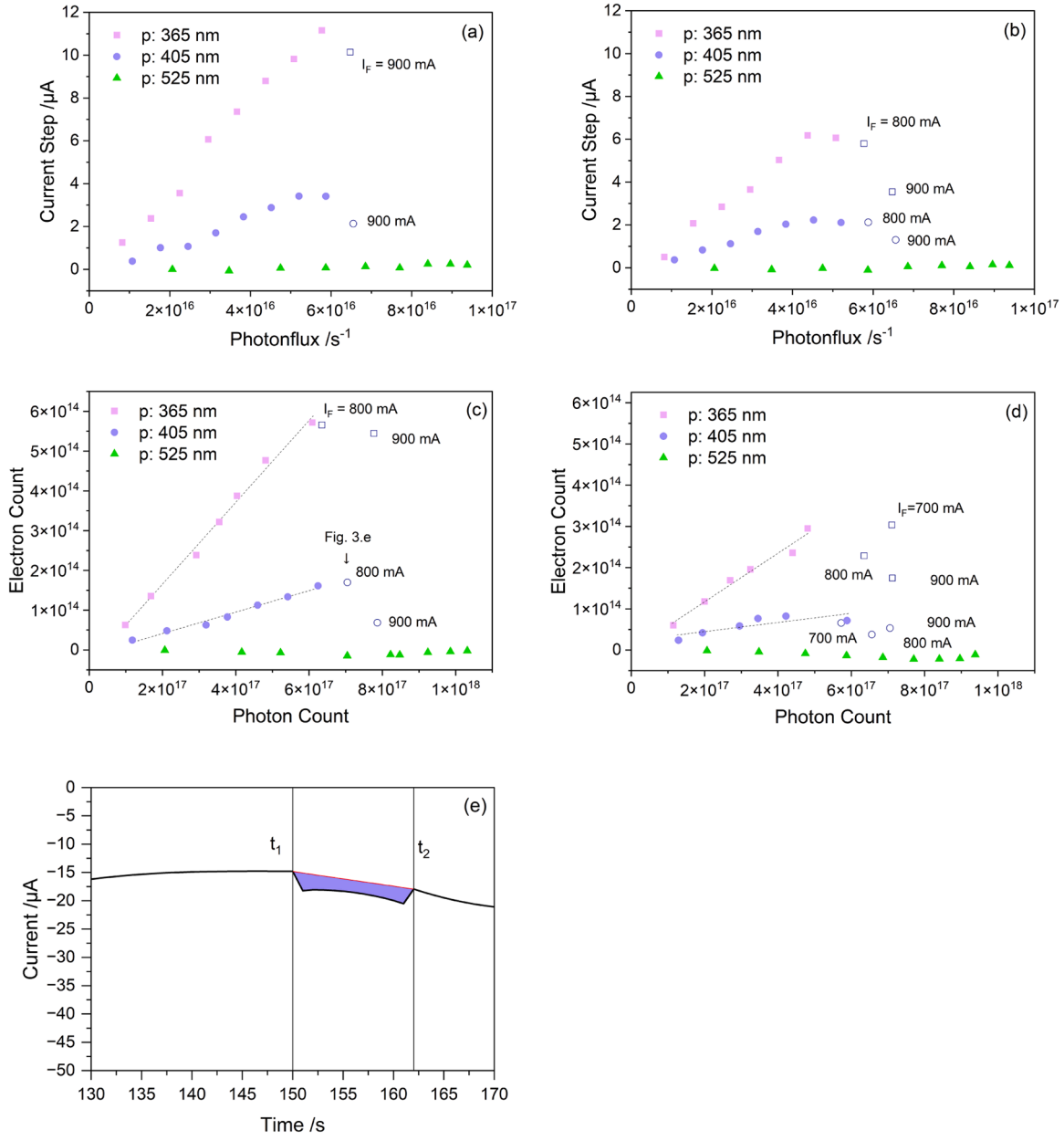

Fig. 4. Current steps as a function of photonfluxes on $Zn_{99.99\%}$ (a) and Z275 (b), respective electron-/photon count plot on $Zn_{99.99\%}$ (c) and Z275 (d) and exemplary integral formation for calculating the electron count (e).

Table 2
Slopes of liner fits of photon-/electron count plots in Fig. 4.c and Fig. 4.d.

	p: 365 nm	p: 405 nm
$Zn_{99.99\%}$ (100–700 mA)	1.03E-03	2.70E-04
Z275 (100–600 mA)	5.89E-04	1.11E-04

quantum yields between 0.1% and 0.3% have been extracted from photocurrent spectra (λ=400 nm) of anodically formed oxides on high purity zinc. The quantum yield in [36] has been described as the quantity of electrons measured in relation to provided photons. Further, the ratios between slopes of UV-light and violet light can be obtained for both substrates. On $Zn_{99.99\%}$ k_{violet} accounts for about 26% of k_{UV}, while on Z275 k_{violet} accounts for about 19% of k_{UV}. In other terms, it is highly likely, that similar phenomena occur on $Zn_{99.99\%}$ and Z275.

A careful examination of the green light experiment reveals a reproducible but minimal current step around zero, that cannot be seen on the scales of Figs. 2–4. Due to its small value compared to the effect created with UV-light and violet light it has been excluded from the discussion so far. Fig. 5 shows enlarged sections of Fig. 2.c, more precisely the current density on $Zn_{99.99\%}$ under green light illumination with a forward current of 700 mA (Fig. 5.a) and 300 mA (Fig. 5.b). The current change triggered by green light is only 2.5% of the current change triggered by UV light, when comparing the experiments with forward currents of 700 mA. However, this value drops to 0.5%, when comparing experiments with similar photonfluxes. Similar photonfluxes are obtained by UV light at 700 mA forward current and green light at 300 mA forward current.

One reason for the observed small effects, is that the spectrum of the green LED eventually includes a small number of photons, having enough energy to generate electron-hole pairs and contribute to the current. This is probably also the reason for the lower but remarkable effect of the violet LED compared to the UV LED. Further explanation might be found in the photoluminescence spectra of ZnO, which are

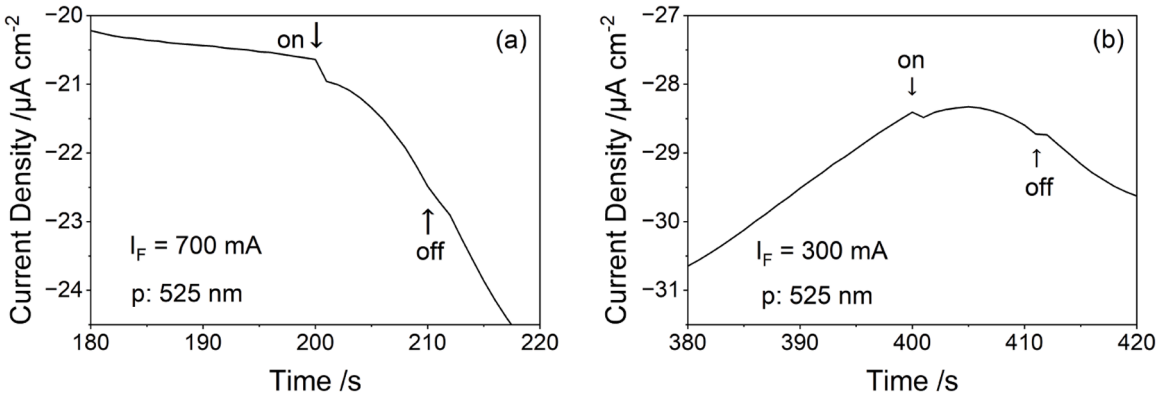

Fig. 5. Current density during potentiostatic condition (−1.05 V vs. E_{ref}) on $Zn_{99,99\%}$ during illumination with green light at forward currents (I_F) of 700 mA (a) and of 300 mA (b).

known to contain a broad emission band in the region of 2.45 eV (green light) [41]. The cause of the emission is not fully understood but has been attributed in the literature to point defect interactions or Cu impurities. One proposed cause is the recombination of a single ionized oxygen vacancy, localized at an energy state close to the conduction band, with a hole in the valence band [18,42]. Conversely, the abrupt influence of green light on the current could also result from an interaction between electrons and point defects of the semiconductor. These processes could influence the conductive properties of ZnO and thus a redox reaction at the semiconductor/electrolyte interface.

The experiments on Z275 were complemented with UV-light measurements on Z100 and ZM120. Differing properties in contrast to Z275 (20 µm and skin-passed) are as follows: Z100 has a zinc layer of 7 µm and provides a non-skin-passed surface, while the ZM120 coating is skin-passed, 9 µm in thickness and has higher content of Al and an additional Mg content.

The respective electron-/photon-count plot was obtained in the already explained manner and is shown in Fig. 6. The linear relation until a saturation level, was obtained on ZM120 and Z100 as well. Moreover the effect increases on Z100 and ZM120. On ZM120 the electron count reaches about double values in contrast to Z275.

Slightly different manifestations of the effect can be caused by the nature of the surface, the degree of reflection and the alloying elements Al and Mg. However, this must be investigated in more detail in a separate research question.

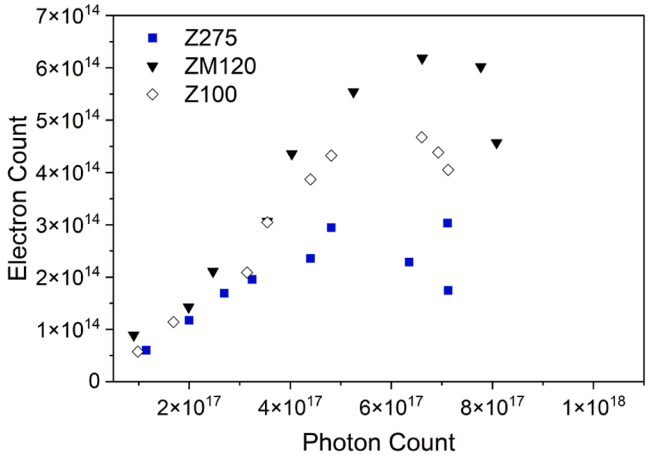

Fig. 6. Electron-/photon count plot of Z275, ZM120 and Z100 obtained through UV-light illumination.

3.3. Ocp measurements

To address the observed photoeffect enhancement on zinc substrates, in the context of delamination, ocp measurements were performed on pre-treated, organic coated Z275 samples during illumination. Experiments performed on 3 h preconditioned samples are pictured in Fig. 7. a–c, while measurements on 114 h preconditioned samples are shown in Fig. 7.d–f. Again, the signal is clearly affected by the onset of the light, with its extent depending on the wavelength. A marked increase in ocp is observed with UV light and violet light, followed by a marked decrease after the light is turned off. In contrast, only slight increases and decreases in ocp can be observed through green light, which are more difficult to distinguish from noise. Possibly, this effect is generated by heating. The observation of an increase in the ocp value under UV and violet light illumination on coated galvanised steel is consistent with the results of similar measurements on bare zinc samples, although different interpretations are given there [22,24,25,28,29].

When comparing Fig. 7.a and d, one can see, that the ocp rises to higher levels, when the preconditioning step is prolonged. More specifically, for UV-light, the ocp change is about 10 mV at 3 h preconditioning compared to 25 mV at 114 h preconditioning. The results suggest that, in comparison to 3 h, a higher amount of ZnO is present after 114 h preconditioning due to corrosion progression. The increase in photo-response on Zn electrodes with increasing immersion time in the electrolyte was also noted in [28], although there it was attributed more to prolonged air exposure.

It is noteworthy, that the ocp rise during UV- and violet light illumination is clearly visible, although the galvanised sample was pre-treated and coated with a 6 µm primer coating. This means, the primers UV protection properties seem to be insufficient in shielding the substrate from the illumination impact of the used LEDs. This can be understood by looking at an UV–Vis transmission spectrum of a 6 µm thick free film of the primer (Fig. 8). The primer contains TiO_2 pigments, which mainly determine the transmission behaviour of the coating. At 3.0 to 3.2 eV (corresponding to approximately 415–390 nm), the band gap of TiO_2 [43] is a little smaller than that of ZnO. The graph also shows the relative spectral power distributions of the LEDs, which were reproduced from the data sheet. The transmission at the corresponding peak-wavelengths is as follows: 365 nm (UV): 5%, 405 nm (violet): 10% and 525 nm (green): 45%. For the phenomenon to occur in the field, a certain UV–Vis permeability of the topcoats is of course a prerequisite. Additional effects due to TiO_2 phases from the pre-treatment were estimated to be small in ocp measurements of regular and pre-treated substrates (not shown here).

Referring to the basic relation of corrosion potential and kinetics, an increase in ocp is caused by an increase of the cathodic reaction or a decrease of the anodic reaction [44]. It is not possible to clearly determine from this experiment which partial reaction is influenced by the

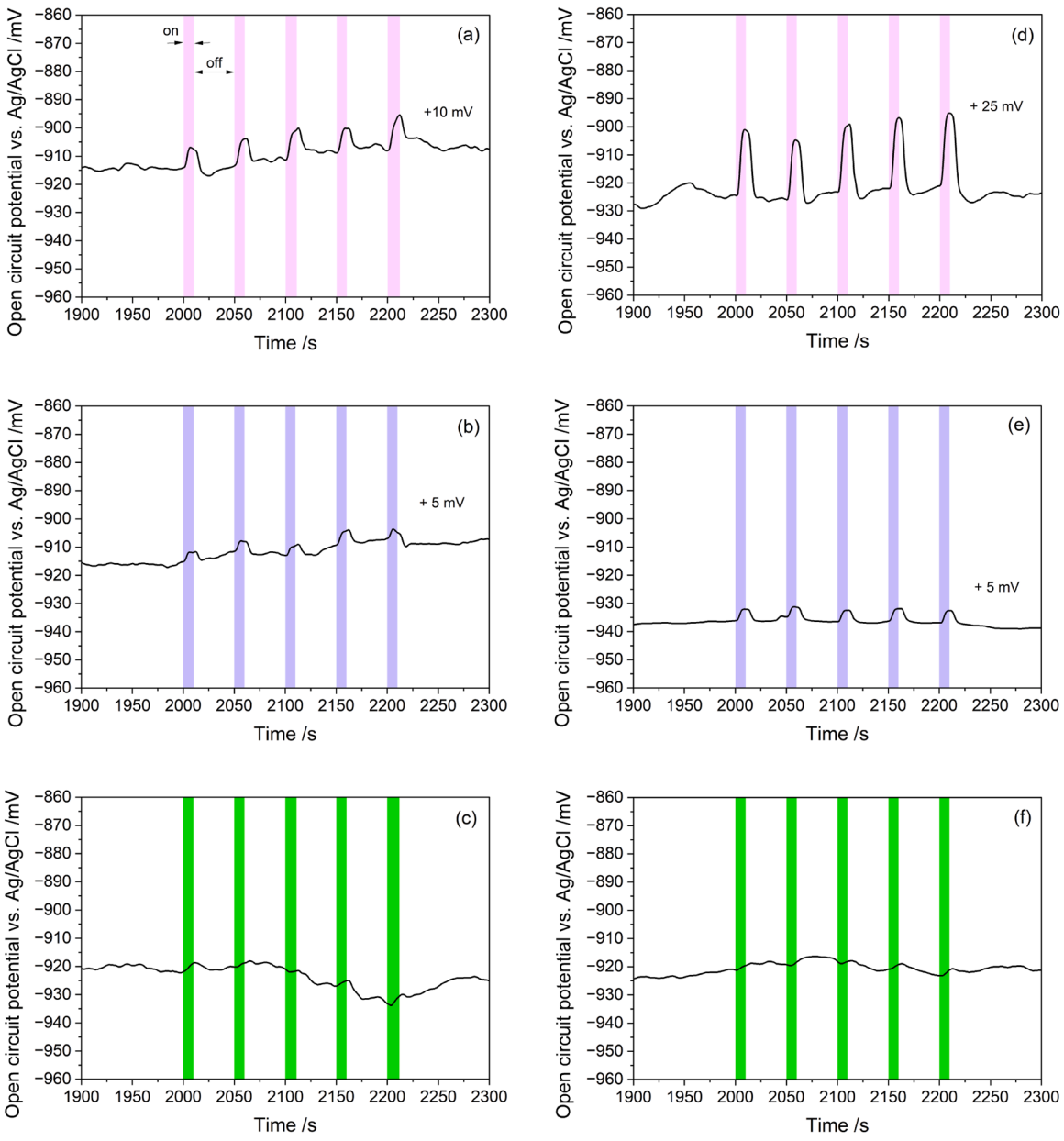

Fig. 7. Ocp measurements on organic coated, pre-treated galvanised steel: after a precondition time of 3 h during 10 s of illumination with UV-light (a), violet light (b) and green light (c) and after a precondition time of 114 h with UV-light (d), violet light (e) and green light (f). All illumination experiments at a forward current (I_F) of 700 mA.

illumination. It can only be said with certainty that there is a photoeffect contribution, even through the primer, under the given conditions.

Looking at the results of the potentiostatic measurements from this perspective, it becomes clear that also here it is not possible to definitively determine which partial reaction is being influenced. The measured current represents a total current that is made up of cathodic and anodic partial currents, even if in the observed case the cathodic ones outweigh the anodic ones. The initial assumption, that the current, which is measured just below the open circuit potential can be attributed to the ORR is possibly too simplistic. Although the results of the potentiostatic measurements and the ocp measurements demonstrate the photoeffect contribution very well, they cannot sufficiently show which reaction is being influenced.

To figure out which reaction(s) involve a photoeffect participation, the flat band potential (E_{FB}) was characterized in Mott-Schottky measurements and used for a mechanistic consideration. CLSV was performed to assess the photo-contribution at different potentials and at high overvoltage.

3.4. Mott-Schottky measurements

Theoretical background on Mott-Schottky measurements can be found in SI and [45]. This method delivers flat band potential (E_{FB}) values, which play a crucial role in understanding the mechanism, as well as donor densities (N_D). Values of E_{FB} and N_D for Z275, ZM120, Z100 and $Zn_{99.99\%}$ in O_2 bubbled $NaHCO_3/H_2O$ (pH ≈ 8.5) were obtained via (Eq. 7) and are given in Table 3.

$$1 \Big/ {C_{sc}}^2 = \frac{2}{e * \varepsilon_0 * \varepsilon * N_D * A^2} * \left(E - E_{FB} - \frac{k * T}{e} \right) \tag{7}$$

The E_{FB} values of the industrial substrates are more positive than the E_{FB} of pure zinc. Taking the experimental error into account, this observation is significant. The consequences of this will be discussed in 3.5. and 3.6. Although the experimental errors for N_D are high, there are

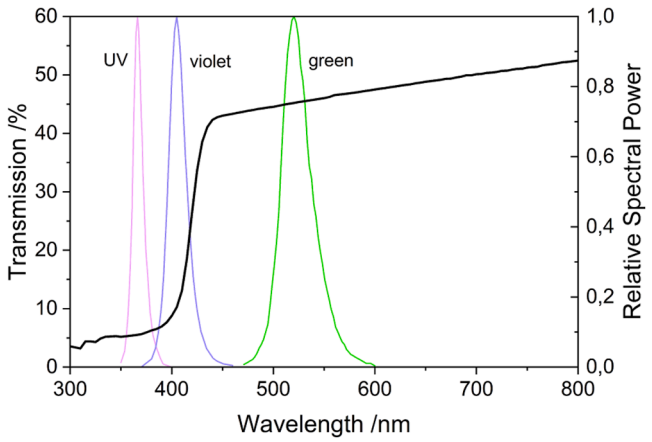

Fig. 8. UV–Vis transmission spectrum of a 6 μm free film primer and relative spectral power distributions of LEDs used.

Table 3
Values for E_{FB} and N_D measured in the dark.

	E_{FB}/V vs. E_{ref}	N_D/cm^{-3}
Z275	−1.08 ± 0.02	1.39E+19 ± 5.31E+18
ZM120	−1.04 ± 0.01	2.67E+18 ± 4.67E+17
Z100	−1.17 ± 0.04	3.13E+19 ± 1.02E+19
$Zn_{99.99\%}$	−1.40 ± 0.05	1.28E+20 ± 2.18E+19

differences in two orders of magnitude, which may correlate with the amount of aluminium or the amount of ZnO formed on the sample as well. Typically, one would expect higher donor densities in Al-doped ZnO. Here however, industrial substrates are regarded in contrast to Al-doped ZnO. As a consequence of the hot dip galvanizing process, industrial substrates provide different phases on the surface (for example $MgZn_2$ on ZM120). Those phases may affect the values for the flatband potential and the donor density in an indeterminable way.

3.5. Mechanistic approach

In the following a mechanism for the observed photoeffect contribution on high purity zinc and galvanised samples is proposed. It must be taken into account, that here an external potential is applied, as this changes the band-bending. The scenario obtained for pure electrolyte contact with no external potential applied can be found discussed in SI.

The point at which no band-bending occurs is called the flatband potential [46] (Fig. 9.a). At the flatbandpotential no space charge exists and up to this point, in the dark, the photocurrent remains almost zero. The set potential in relation to the flatband potential defines the direction of band bending: A set potential more negative than the flatband potential creates a downward bend [36] (Fig. 9.b), while a set potential more positive than the flatband potential creates an upward bend (Fig. 9.c).

A certain band-bending, and therefore a potential unequal the flatband potential is needed to obtain a separation of photo-generated electrons and holes within the space-charge layer and their contribution to redox reactions. Directly at the flatband-potential mainly recombination of generated charge carriers takes place.

When illumination with photons of sufficient energy (maybe accompanied by increased temperature) is provided, band-gap transition is enabled, and electron-hole pairs are generated. The direction of band-bending determines whether electrons flow to the substrate (cathodic protection) or the electrolyte: Considering the direction of the Fermi scale, electrons will naturally flow downwards the energy bands, while holes flow upwards [46].

In a situation like in Fig. 9.b electrons migrate to the electrolyte. This situation is needed for the enhancement of the ORR, as proposed in this work. The remaining holes on the contrary migrate towards the semiconductor or metal due to polarization and recombine with electrons from the external circuit. Electron/hole pairs, from which electrons are not consumed by ORR will recombine in the surface space charge layer. Solely in a situation like in Fig. 9.b, electrons could be consumed by the available O_2 in the ORR. When the energy level of the CB directly at the interface falls below the E_F of the semiconductor, additional metal dissolution is provoked [36].

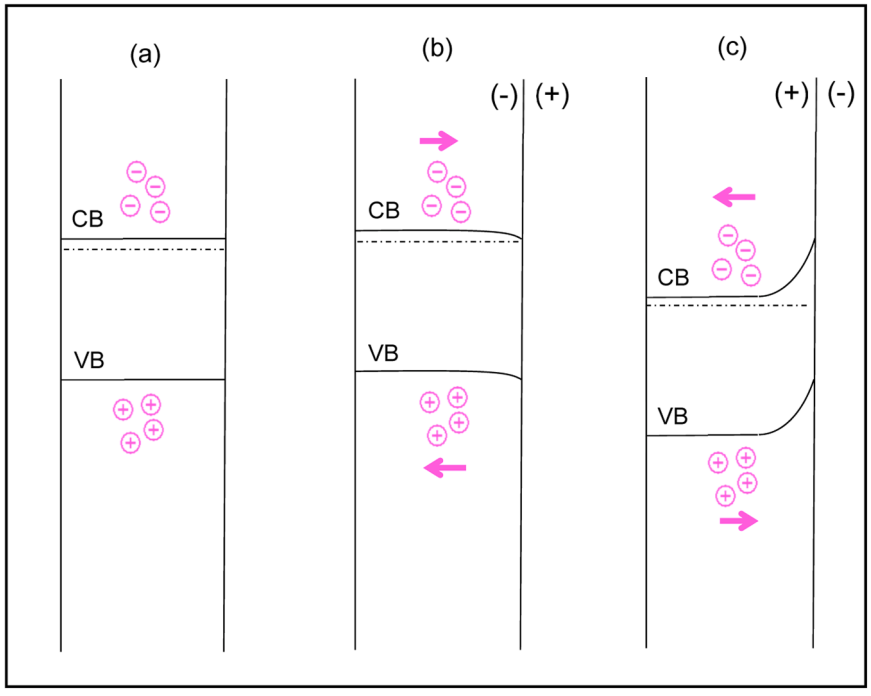

Fig. 9. Proposed mechanism for the observed photo-effect contribution under a set potential equal (a), below (b) and above E_{FB} (c) plus illumination of energy $>E_g$ (bandgap energy).

The knowledge of the flat band potential values from the Mott-Schottky measurements and the theoretical considerations on the band structure enable to determine the band bending in the CLSV measurements given in 3.6. From this it can be assessed whether an essential mechanistic prerequisite for ORR amplification is given.

3.6. Light chopped linear sweep voltammetry

Fig. 10.a shows the linear sweep curves on Z275 while illuminating with chopped UV-, violet and green light. Light chopping basically created data alternating between two current curves. In one curve light is present, in the other one light is absent. Those two curves cannot be distinguished on the scale of Fig. 10.a (Z275), as they only differ slightly in contrast to the absolute current measured. Fig. 10.(a-1) gives therefore an enlarged section of the measured current in a dot diagram with the corresponding light chopping scheme. The difference between the current during illumination and the current without illumination (ΔI) is displayed in Fig. 10.b as a function of the potential.

Fig. 10.b extends the validity of the already observed wavelength dependence to a large potential range. For UV-light and violet light measurements, the current step is always negative. This is a consequence of the shift to lower currents above the ocp and a shift to higher currents below the ocp. The fluctuation that is obtained with green light at around −1.45 V vs. E_{ref} is not necessarily a relevant observation but rather a consequence of the calculation.

The evolution of the current step over the potential shows two maxima: The one at −1.40 to −1.45 V aligns with the Zn^{2+}-reduction peak of the polarization curve and is interpreted as reduction of Zn ions in the oxide/hydroxide/carbonate layer [5]. Also, this reaction is light-enhanced and regarded detrimental for adhesion as well. Below the Zn^{2+}-reduction peak, the absolute current step starts to diminish, which corresponds well with the degradation of ZnO through the starting hydrogen evolution reaction.

The maxima at around −1.10 V vs. E_{ref}. is in the potential region, where the ORR was initially assumed to be found. An intensification of the ORR according to the determined flatband potential would start to become possible in the range of this maximum. The polarization curve in Fig. 10.a however shows a nearly flat part in that specific potential region. This means that the current is actually limited by diffusion. An enhancement of the ORR by the photoeffect would therefore only be conceivable if, for example, the two-step ORR (Eq. 2) changes to the four-step ORR (Eq. 1). In this case the current could not be more than doubled by the illumination.

Fig. 11 shows the ratio of the current step to the total current in percentage as a function of the potential for Z275 in enriched O_2 (Fig. 11.a) and in Ar atmosphere (Fig. 11.b) and for $Zn_{99.99\%}$ in enriched O_2 (Fig. 11.c). The measurement of Z275 in enriched O_2 (Fig. 11.a) shows a characteristic feature in the potential range of approx. −1.10 V vs E_{ref}. The position of the feature in the graph aligns well with the documented potential range of the 2-electron ORR pathway on $Zn(OH)_2$ covered Zn/Al-coatings at pH 9.6 [7] and on oxide-covered zinc in NaCl [5]. The characteristic feature is missing in Ar-atmosphere on Z275 (Fig. 11.b), which proofs the photo-enhancement of the ORR. For $Zn_{99.99\%}$ in enriched O_2, the characteristic maximum is missing as well, which is consistent with the unfulfilled condition of band bending according to Fig. 9. for ORR amplification. An upward band bending is created, and electrons flow to the metal side. The additional current due to the illumination is a maximum of 20% in the corresponding potential range for Z275 (see Fig. 11.a). This means that the assumption of the 2- to 4-electron ORR shift can be pursued further. For Z275 and $Zn_{99.99\%}$, the fraction of the maximum current generated by light is about 10% in the range of −1.40 V to −1.45 V vs. E_{ref}. In any situation where band bending as in Fig. 9.c occurs, a decrease in Zn-oxidation due to hole migration to the surface is possible.

4. Conclusions

Main results can be expressed as follows:

- During cathodic overvoltage, illumination on both $Zn_{99.99\%}$ and Z275 instantaneously increased currents to extents depending on the wavelength. The wavelength dependence is in accordance with the

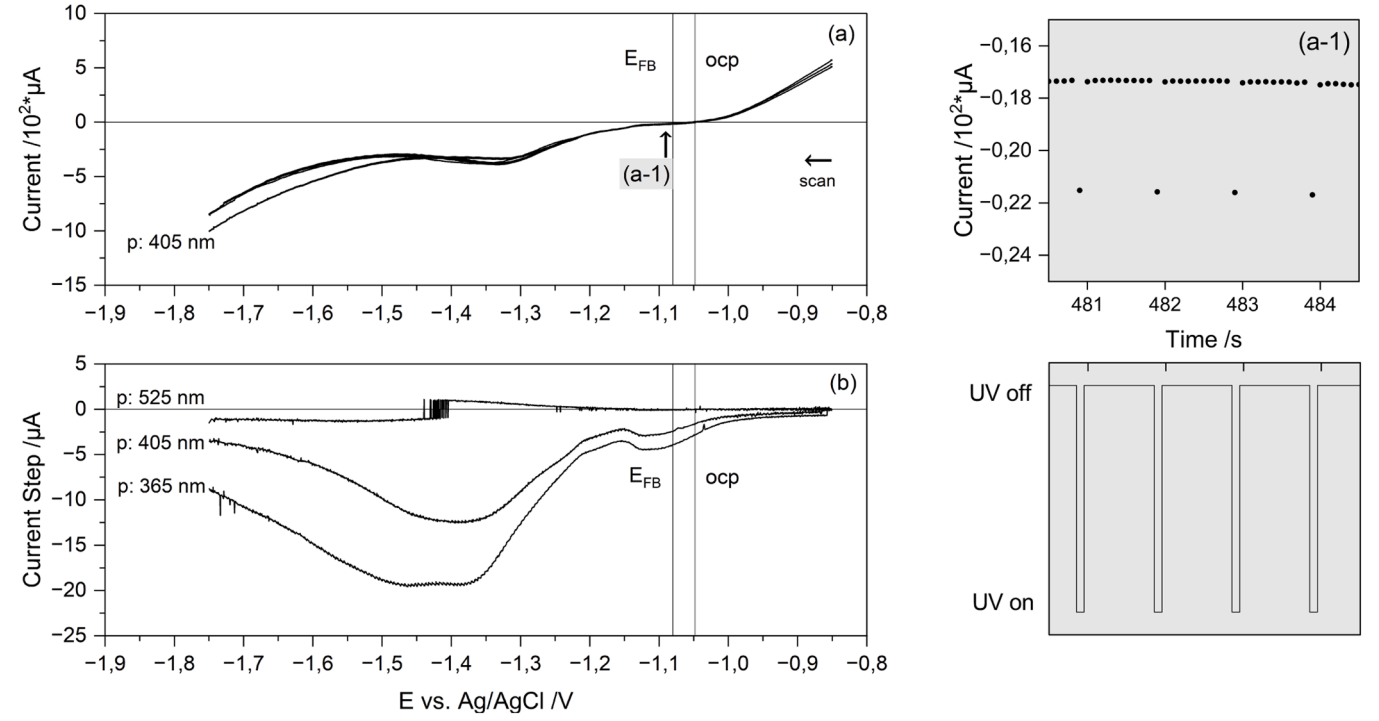

Fig. 10. Linear sweep voltammetry curves on Z275 under chopped UV-, violet and green light illumination (a) and corresponding generated current step (b) – (a-1) shows the time-related light scheme and a detailed section of the measured current when chopping with UV light.

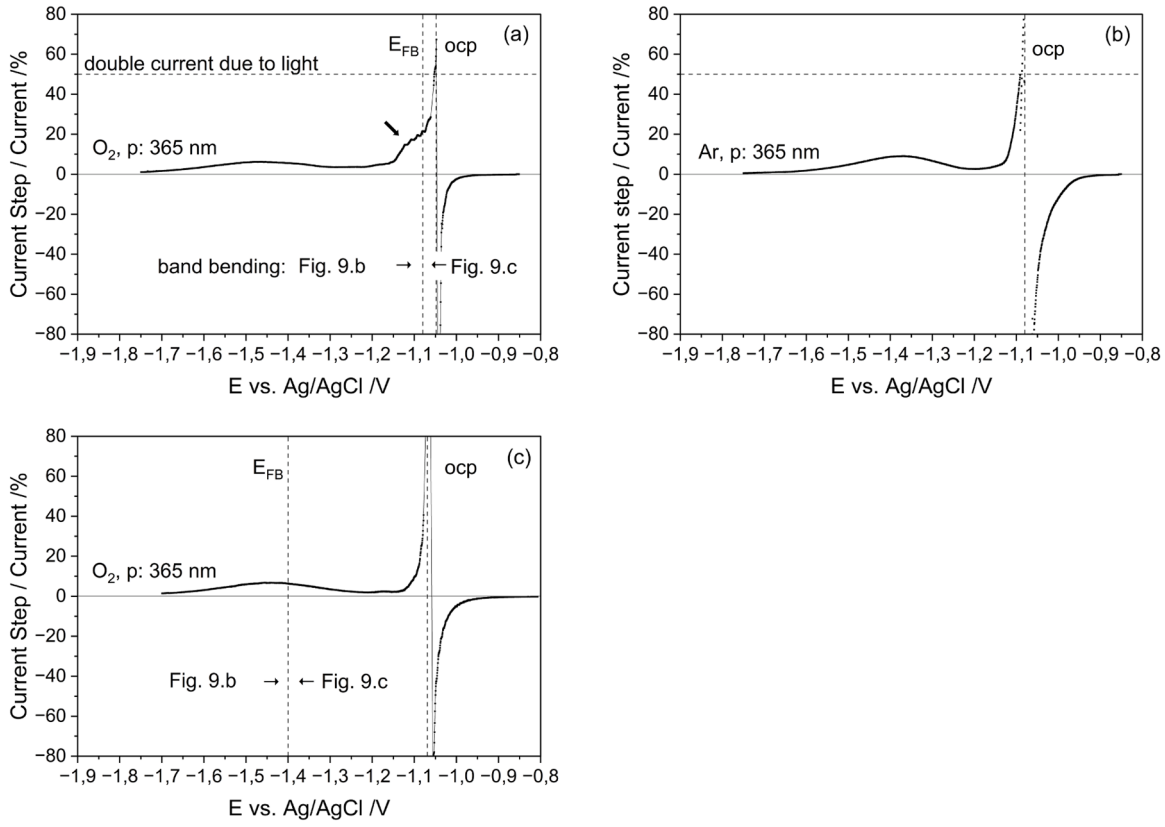

Fig. 11. Ratio of the current step generated by UV-light to the total current as a function of the potential on Z275 in enriched O_2 (a), on Z275 in Ar (b) and on $Zn_{99,99\%}$ in enriched O_2 (c).

bandgap of ZnO. Almost zero effect was obtained, when conducting the experiment with non-sufficient energy of green light. The effect varied proportional with intensity, when conducting the experiments with UV-light and violet light. A linear relation was obtained between the photon flux and the additionally consumed electrons until a certain saturation level. Via systematic wavelength and intensity variation, the results provide a clear evidence of photoeffect involvement.

- A time-shifted temperature effect on $Zn_{99,99\%}$ and industrial Zn-samples has been observed as well, which might have different origins, however.
- The study of three industrial galvanised samples revealed similar behaviour in comparison with $Zn_{99,99\%}$. This underlines the importance of the described phenomenon not only on high purity laboratory samples but also in application.
- The ocp values of the coated and pre-treated galvanised samples increased during the illumination period, which would also be expected for ORR enhancement. The extent again depended on the wavelength of the light-source in accordance with the bandgap of ZnO. Additional ocp increase was observed after prolonged preconditioning time in the electrolyte during UV-light illumination.
- First reflections on the mechanism are provided, considering a theoretical approach, flat band potential values and CLSV. According to this, the phenomenon observed on Z275, but not on $Zn_{99,99\%}$, can be associated with ORR intensification. However, results from CLSV suggest that other reactions in addition to ORR may be influenced by the photoeffect and contribute to delamination. The original research question of ORR amplification should be further investigated using methods such as the rotating disk electrode.
- The obtained findings suggest a plausible connection between cathodic delamination and both the photoeffect on ZnO, as well as its temperature dependant semiconducting properties. This relation has not been considered so far and might be a starting point for further investigating disbondment failure of organic coated galvanised steel exposed to elevated temperature and UV-impact by sunlight.

CRediT authorship contribution statement

Anna Aspalter: Conceptualization, Methodology, Validation, Formal analysis, Investigation, Writing – original draft, Visualization. **Roland Braidt:** Conceptualization, Methodology, Formal analysis, Resources, Writing – review & editing. **Jiri Duchoslav:** Investigation. **Bernhard Strauß:** Conceptualization, Resources, Writing – review & editing, Project administration. **Günter Fafilek:** Conceptualization, Methodology, Resources, Writing – review & editing, Supervision.

Declaration of competing interest

The authors declare that they have no known competing financial interests or personal relationships that could have appeared to influence the work reported in this paper.

Data availability

Data will be made available on request.

Acknowledgements

This work was financially supported by the Austrian Research Promotion Agency (FFG, Project No. FO9999 06791). J.D. gratefully acknowledges the government of Upper Austria for financial support within the project “ASAES”. The authors acknowledge TU Wien Bibliothek for financial support through its Open Access Funding

Programme.

Supplementary materials

Supplementary material associated with this article can be found, in the online version, at doi:10.1016/j.electacta.2024.144453.

References

[1] W. Fürbeth, M. Stratmann, The delamination of polymeric coatings from electrogalvanised steel – a mechanistic approach, Corros. Sci. 43 (2001) 207–227, https://doi.org/10.1016/S0010-938X(00)00047-0.

[2] R. Hausbrand, M. Stratmann, M. Rohwerder, Corrosion of zinc–magnesium coatings: mechanism of paint delamination, Corros. Sci. 51 (2009) 2107–2114, https://doi.org/10.1016/j.corsci.2009.05.042.

[3] C.M. Griffiths, N. Wint, G. Williams, H.N. McMurray, The contribution of Zn(II) and phosphate anions to the inhibition of organic coating cathodic disbondment on galvanised steel by zinc phosphate pigment, Corros. Sci. 198 (2022) 110111, https://doi.org/10.1016/j.corsci.2022.110111.

[4] K. Ogle, S. Morel, N. Meddahi, An electrochemical study of the delamination of polymer coatings on galvanized steel, Corros. Sci. 47 (2005) 2034–2052, https://doi.org/10.1016/j.corsci.2004.08.017.

[5] A.P. Yadav, A. Nishikata, T. Tsuru, Oxygen reduction mechanism on corroded zinc, J. Electroanalytical Chem. 585 (2005) 142–149, https://doi.org/10.1016/j.jelechem.2005.08.007.

[6] J.D. Yoo, P. Volovitch, A. Abdel Aal, C. Allely, K. Ogle, The effect of an artificially synthesized simonkolleite layer on the corrosion of electrogalvanized steel, Corros. Sci. 70 (2013) 1–10, https://doi.org/10.1016/j.corsci.2012.10.024.

[7] H. Dafydd, D.A. Worsley, H.N. McMurray, The kinetics and mechanism of cathodic oxygen reduction on zinc and zinc–aluminium alloy galvanized coatings, Corros. Sci. 47 (2005) 3006–3018, https://doi.org/10.1016/j.corsci.2005.05.036.

[8] M. Prestat, F. Vucko, B. Lescop, S. Rioual, F. Peltier, D. Thierry, Oxygen reduction at electrodeposited ZnO layers in alkaline solution, Electrochim. Acta 218 (2016) 228–236, https://doi.org/10.1016/j.electacta.2016.09.050.

[9] H. Leidheiser, W. Wang, L. Igetoft, The mechanism for the cathodic delamination of organic coatings from a metal surface, Prog. Org. Coat. 11 (1983) 19–40, https://doi.org/10.1016/0033-0655(83)80002-8.

[10] S. Bhargava, M. Kubota, R.D. Lewis, S.G. Advani, A.K. Prasad, J.M. Deitzel, Ultraviolet, water, and thermal aging studies of a waterborne polyurethane elastomer-based high reflectivity coating, Prog. Org. Coat. 79 (2015) 75–82, https://doi.org/10.1016/j.porgcoat.2014.11.005.

[11] J. Mallégol, M. Poelman, M.-G. Olivier, Influence of UV weathering on corrosion resistance of prepainted steel, Prog. Org. Coat. 61 (2008) 126–135, https://doi.org/10.1016/j.porgcoat.2007.09.026.

[12] F.E. Bedoya, L.M. Gallego, A. Bermúdez, J.G. Castaño, F. Echeverría, J.A. Calderón, J.G. Maya, New strategy to assess the performance of organic coatings during ultraviolet–condensation weathering tests, Electrochim. Acta 124 (2014) 119–127, https://doi.org/10.1016/j.electacta.2013.09.064.

[13] D. Persson, G. Heydari, C. Edvinsson, P.E. Sundell, Depth-resolved FTIR focal plane array (FPA) spectroscopic imaging of the loss of melamine functionality of polyester melamine coating after accelerated and natural weathering, Polym. Test. 86 (2020) 106500, https://doi.org/10.1016/j.polymertesting.2020.106500.

[14] F. Deflorian, S. Rossi, L. Fedrizzi, C. Zanella, Comparison of organic coating accelerated tests and natural weathering considering meteorological data, Prog. Org. Coat. 59 (2007) 244–250, https://doi.org/10.1016/j.porgcoat.2006.09.036.

[15] F. Deflorian, S. Rossi, M. Fedel, Organic coatings degradation: comparison between natural and artificial weathering, Corros. Sci. 50 (2008) 2360–2366, https://doi.org/10.1016/j.corsci.2008.06.009.

[16] V.A. Coleman, C. Jagadish, Basic Properties and Applications of ZnO, in: C. Jagadish (Ed.), Zinc Oxide bulk, Thin Films and nanostructures: Processing, Properties and Applications, 1st ed., Elsevier, Amsterdam, 2006, pp. 1–20.

[17] T.C. Collins, R.J. Hauenstein, Fundamental Properties of ZnO, in: C.W. Litton (Ed.), Zinc Oxide Materials For Electronic and Optoelectronic Device Applications, Wiley, Chichester, 2011, pp. 1–28.

[18] Z.L. Wang, Zinc oxide nanostructures: growth, properties and applications, J. Phys.: Condens. Matter 16 (2004) R829–R858, https://doi.org/10.1088/0953-8984/16/25/R01.

[19] Y. Liu, Z. Zhu, Y. Cheng, An in-depth study of photocathodic protection of SS304 steel by electrodeposited layers of ZnO nanoparticles, Surface Coat. Technol. 399 (2020) 126158, https://doi.org/10.1016/j.surfcoat.2020.126158.

[20] Y. Liu, Z. Zhu, Y. Cheng, B. Wei, Y. Cheng, Effect of electrodeposition temperature on the thin films of ZnO nanoparticles used for photocathodic protection of SS304, J. Electroanalytical Chem. 881 (2021) 114945, https://doi.org/10.1016/j.jelechem.2020.114945.

[21] M. Li, S. Luo, P. Wu, J. Shen, Photocathodic protection effect of TiO2 films for carbon steel in 3% NaCl solutions, Electrochim. Acta 50 (2005) 3401–3406, https://doi.org/10.1016/j.electacta.2004.12.031.

[22] M. Sun, Z. Chen, Y. Bu, J. Yu, B. Hou, Effect of ZnO on the corrosion of zinc, Q235 carbon steel and 304 stainless steel under white light illumination, Corros. Sci. 82 (2014) 77–84, https://doi.org/10.1016/j.corsci.2013.12.022.

[23] Y. Bu, J.-P. Ao, A review on photoelectrochemical cathodic protection semiconductor thin films for metals, Green Energy Environ. 2 (2017) 331–362, https://doi.org/10.1016/j.gee.2017.02.003.

[24] Q. Li, W. Li, M. An, Sunlight induced photoelectrochemical anticorrosion effect of corrosion product layers on electrogalvanized steel in simulated seawater, Electrochem. Commun. 90 (2018) 39–42, https://doi.org/10.1016/j.elecom.2018.03.010.

[25] Q. Li, D. Zeng, M. An, Elevating the photo-generated cathodic protection of corrosion product layers on electrogalvanized steel through nano-electrodeposition, Chem. Phys. Lett. 722 (2019) 1–5, https://doi.org/10.1016/j.cplett.2019.02.030.

[26] P. Spathis, I. Poulios, The corrosion and photocorrosion of zinc and zinc oxide coatings, Corros. Sci. 37 (1995) 673–680, https://doi.org/10.1016/0010-938X(95)80001-8.

[27] A.L. Rudd, C.B. Breslin, Photo-induced dissolution of zinc in alkaline solutions, Electrochim. Acta 45 (2000) 1571–1579, https://doi.org/10.1016/S0013-4686(99)00322-9.

[28] E. Juzeliūnas, P. Kalinauskas, A. Stankevičiūtė, A. Sudavičius, A. Survila, Study of zinc oxygen corrosion kinetics in neutral solution under laser illumination, Corrosion 51 (1995) 672–678, https://doi.org/10.5006/1.3293629.

[29] P. Kalinauskas, I. Valsiūnas, M. Samulevičien≐, E. Juzeliūnas, Zinc photo-corrosion in neutral solutions, Corros. Sci. 43 (2001) 2083–2092, https://doi.org/10.1016/S0010-938X(01)00013-0.

[30] E.A. Thompson, T.D. Burleigh, Accelerated corrosion of zinc alloys exposed to ultraviolet light, Corrosion Eng. Sci. Technol. 42 (2007) 237–241, https://doi.org/10.1179/174327807X214581.

[31] A. Nazarov, E. Diler, D. Persson, D. Thierry, Electrochemical and corrosion properties of ZnO/Zn electrode in atmospheric environments, J. Electroanalytical Chem. 737 (2015) 129–140, https://doi.org/10.1016/j.jelechem.2014.07.029.

[32] J. Yang, K. Liu, X. Chen, D. Shen, Recent advances in optoelectronic and microelectronic devices based on ultrawide-bandgap semiconductors, Prog. Quantum. Electron. 83 (2022) 100397, https://doi.org/10.1016/j.pquantelec.2022.100397.

[33] S. Heo, E. Cho, H.-I. Lee, G.S. Park, H.J. Kang, T. Nagatomi, P. Choi, B.-D. Choi, Band gap and defect states of MgO thin films investigated using reflection electron energy loss spectroscopy, AIP. Adv. 5 (2015), https://doi.org/10.1063/1.4927547.

[34] J. López, E. Solorio, H.A. Borbón-Nuñez, F.F. Castillón, R. Machorro, N. Nedev, M. H. Farías, H. Tiznado, Refractive index and bandgap variation in Al2O3-ZnO ultrathin multilayers prepared by atomic layer deposition, J. Alloys. Compd. 691 (2017) 308–315, https://doi.org/10.1016/j.jallcom.2016.08.271.

[35] J. Cunningham, Chapter 3 Radiation and Photoeffects at Gas/Solid Interfaces, in: Simple Processes At the Gas-Solid Interface, Elsevier, 1984, pp. 291–427.

[36] T.D. Burleigh, Anodic photocurrents and corrosion currents on passive and active-passive metals, Corrosion 45 (1989) 464–472, https://doi.org/10.5006/1.3582045 [Dataset].

[37] O. Coddington, J.L. Lean, P. Pilewskie, M. Snow, C. Lindholm, D. Lindholm, NOAA CDR Program, NOAA Climate Data Record (CDR) of solar spectral irradiance (SSI), NRLSSI Version 2.1. https://doi.org/10.7289/V53776SW.

[38] P.J. Mohr, D.B. Newell, B.N. Taylor, CODATA recommended values of the fundamental physical constants: 2014, Rev. Mod. Phys. 88 (2016), https://doi.org/10.1103/RevModPhys.88.035009.

[39] D.C. Look, Doping and Defects in ZnO, in: C. Jagadish (Ed.), Zinc Oxide bulk, Thin Films and nanostructures: Processing, Properties and Applications, 1st ed., Elsevier, Amsterdam, 2006, pp. 21–42.

[40] A.E. Bohe, J.R. Vilche, K. Jüttner, W.J. Lorenz, W. Paatsch, Investigations of the semiconductor properties of anodically formed passive layers on Zn and of ZnO single crystals in different aqueous electrolytes by EIS, Electrochim. Acta 34 (1989) 1443–1448, https://doi.org/10.1016/0013-4686(89)87186-5.

[41] B.K. Meyer, H. Alves, D.M. Hofmann, W. Kriegseis, D. Forster, F. Bertram, J. Christen, A. Hoffmann, M. Straßburg, M. Dworzak, U. Haboeck, A.V. Rodina, Bound exciton and donor–acceptor pair recombinations in ZnO, phys. Stat. Sol. (b) 241 (2004) 231–260, https://doi.org/10.1002/pssb.200301962.

[42] Ü. Özgür, H. Morkoç, Optical properties of ZnO and related alloys, in: C. Jagadish (Ed.), Zinc Oxide bulk, Thin Films and nanostructures: Processing, Properties and Applications, 1st ed., Elsevier, Amsterdam, 2006, pp. 175–239.

[43] S. Tosoni, G. Di Liberto, G. Pacchioni, Structural and electronic properties of TiO2 from first principles calculations. Titanium Dioxide (Tio_2) and Its Applications, Elsevier, 2021, pp. 67–85.

[44] X.G. Zhang, Corrosion and Electrochemistry of Zinc, 1st ed., Plenum Press, New York, 1996.

[45] K. Gelderman, L. Lee, S.W. Donne, Flat-Band Potential of a Semiconductor: using the Mott–Schottky Equation, J. Chem. Educ. 84 (2007) 685, https://doi.org/10.1021/ed084p685.

[46] C.H. Hamann, W. Vielstich, Elektrochemie, 4th ed., Wiley-VCH-Verlag GmbH & Co. KGaA, Weinheim, 2005.